Ultrasonics Sonochemistry 94 (2023) 106341

Contents lists available at ScienceDirect

Ultrasonics Sonochemistry

journal homepage: www.elsevier.com/locate/ultson

Ultrasound-assisted air-jet spinning of silk fibroin-soy protein nanofiber composite biomaterials

Futian Yang [a,b], Fang Wang [a,b,*], Janine Mazahreh [c,d], Xiao Hu [c,e,*]

[a] Center of Analysis and Testing, Nanjing Normal University, Nanjing 210023, PR China
[b] School of Chemistry and Materials Science, Nanjing Normal University Jiangsu, Nanjing 210023, PR China
[c] Department of Physics and Astronomy, Rowan University, Glassboro, NJ 08028, USA
[d] Department of Chemistry and Biochemistry, Rowan University, Glassboro, NJ 08028, USA
[e] Department of Molecular and Cellular Biosciences, Rowan University, Glassboro, NJ 08028, USA

ARTICLE INFO

Keywords:
Ultrasound
Air jet spinning
Protein
Nanofibers
Crystal structure
SDGs

ABSTRACT

Ultrasound utilizes a non-radiation technology that can meet modern standards to gain access to cheap, reliable and sustainable modern energy. Ultrasound technology can be implemented in the field of biomaterials for its exceptional potential in controlling the shape of nanomaterials. This study presents the first example of the production of soy and silk fibroin protein composite nanofibers in various ratios via combining ultrasonic technology with air-spray spinning. Characterization of ultrasonic spun nanofibers was performed by scanning electron microscopy (SEM), Fourier-transform infrared spectroscopy (FTIR), X-ray powder diffraction (XRD), differential scanning calorimetry (DSC), thermogravimetric (TG) analysis, water contact angle, water retention, enzymatic degradation, and cytotoxicity assays. The effects that adjustments on the ultrasonic time have on the surface morphology, structures, thermal properties, hydrophilicity, water-uptake, bio-enzyme degradability, mechanical properties, and cytocompatibility of the material were examined. It was discovered that as the sonication time increased from 0 to 180 min, the beading phenomenon disappeared, forming nanofibers with uniform diameter and porosity; while the content of β-sheet crystals in the composites and their thermal stability gradually increased, the materials glass transition temperature decreased, and preferred mechanical properties were obtained. Additional studies show that the hydrophilicity, water retention capacity and enzymatic degradation rate were also enhanced by ultrasound, providing a favorable environment for cell attachment and proliferation. This study highlights the experimental and theoretical methods for ultrasound assisted air-jet spinning of biopolymer nanofibrous materials with tunable properties and high biocompatibility, which provide a wide range of applications in wound dressings and drug-carrying systems. This work shows great potential for a direct road to sustainable development of protein based fibers in the industry, thus promoting economic growth, and improving the health of the general population and well-being of wounded patients worldwide.

1. Introduction

Ultrasound technology has emerged as an important tool for the development and application of advanced biological nanomaterials [1-3]. This technology is highly efficient, easily operated, and economically viable [1,2], making it a cheap and reliable source of modern energy. Ultrasound generates a series of dense and alternating longitudinal waves through medium propagation to construct a sound field that can be a divergent, planar, or focused. This promotes the transmission of mechanical vibration energy [4]. Ultrasonic cavitation can alter physical and chemical properties of a material, as well as the modify the overall structure [5]. For example, Xu *et al.* [6] obtained nanoscale CPS (hydroxyapatite) powder using ultrasonic treatment for bone defect repair. Smritilekha *et al.* [7] synthesized nanoparticles with a glycoside backbone by ultrasonic radiation for drug delivery. Sangram *et al.* [8] found that the use of ultrasound transformed silk fibroin protein from its random coil conformation to β-sheets conformation. The results suggested that the ultrasound processed material had a controllable crystallinity and degradation rate. Other studies have found that ultrasound can promote stabilization of the antioxidant and antibacterial activities

* Corresponding authors at: Center of Analysis and Testing, Nanjing Normal University, Nanjing 210023, PR China (F. Wang); Department of Physics and Astronomy, Rowan University, Glassboro, NJ 08028, USA (X. Hu).
E-mail addresses: wangfang@njnu.edu.cn (F. Wang), hu@rowan.edu (X. Hu).

https://doi.org/10.1016/j.ultsonch.2023.106341
Received 23 November 2022; Received in revised form 27 January 2023; Accepted 17 February 2023
Available online 20 February 2023

Table 1
Examples of some research that advances the SDGs.

The Focus of the Study	Key Points	SDGs and Targets	Countries of affiliation (authors)	Reference (in the manuscript)
Use of ultrasonication to simplify the extraction process of the silk peptide under low salt conditions at 20 °C, instead of using the conventional conditions of high salt and temperature.	•Ultrasound treatment on silk decreased solvent use and increased protein yield. •Silk peptide treated with ultrasound and papain had suppressed p-ERK, COX-2, and PGE2 in skin inflammation.	•SDG-3: Ensure healthy lives and promote well-being for all at all ages. Target 3.9 •SDG-12: Ensure Sustainable consumption and production patterns. Target 12.2	Republic of Korea	[1]
The physical properties and structure of silk fibroin protein can be fine-tuned by ultrasonic treatment at different time and power.	•The structure and properties of proteins are adjusted by the power and timing of an efficient and easy to operate ultrasonic technique. •The biological reaction of the protein material can be controlled by ultrasonic treatment.	•SDG-7: Affordable, reliable, and sustainable access to modern energy for everyone. Target 7.a •SDG-12: Ensuring sustainable consumption and production patterns. Target 12.2 •SDG-3: Ensure healthy lives and promote well-being for all at all ages. Target 3.9	China	[2]
Ultrasonic technology is applied in the field of food to study how different conditions affect the functional properties of proteins.	•Ultrasonic technology as a "green technology" can be used to improve the functional properties of proteins.	•SDG-2: Ending hunger, achieving food security, improving nutrition and promoting sustainable agriculture. Target 2.1 SDG-7: Affordable, reliable, and sustainable access to modern energy for everyone. Target 7.a	Mexico	[3]
Effects of ultrasonic techniques on agglomeration, degradation, morphology, structure and mechanical properties of novel materials of natural polymers.	•The ultrasonic cavitation effect the modulates, structure, thermochemical interactions and biological effects of natural polymer materials, thereby enabling physical manipulation of biocompatibility and green polymer material structures.	•SDG-3: Ensure healthy lives and promote well-being for all at all ages. Target 3.9 •SDG-7: Affordable, reliable, and sustainable access to modern energy for everyone. Target 7.1	China	[4]
Effects of high-intensity sonication on aggregated β-glycine and glycine fractions in soybean.	•High-intensity ultrasound can change the structure and physicochemical of soybean components, leading to the improvement of the application of ultrasound technology in the soybean protein industry.	•SDG-2: Ending hunger, achieving food security, improving nutrition and promoting sustainable agriculture. Target 2.1 •SDG-7: Affordable, reliable, and sustainable access to modern energy for everyone. Target 7.1	China	[5]
The crystallization and morphology of Si-apatite precursors synthesized by water precipitation with or without ultrasonic assistance were studied.	•Nanocrystalline CPS powders were successfully obtained under ultrasound-assisted conditions, exhibited better *in vitro* bioactivity and osteogenic activity, and are promising in bone tissue regeneration applications.	•SDG-7: Affordable, reliable, and sustainable access to modern energy for everyone. Target 7.1	China	[6]
Sonication to synthesize carbohydrate-coated nanoparticles for use in optical sensing, packaging materials, agricultural products, and food.	•Ultrasonic technology can control chemical reactions, the production of sensors, the improvement of optical properties, the development of packaging materials, and the development of new technologies for the agricultural and food industries. •It can promote the surface modification of carbohydrate-coated nanoparticles, enhance particle size, prevent caking and shorten reaction time.	•SDG-2: Ending hunger, achieving food security, improving nutrition and promoting sustainable agriculture. Target 2.1 •SDG-7: Affordable, reliable, and sustainable access to modern energy for everyone. Target 7.a •SDG-12: Adopt sustainable consumption and production patterns. Target 12.a	India	[7]
The effect of ultrasonic treatment on the transformation behavior and physicochemical properties of silk fibroin sol-gel was studied.	•The degree of β-sheet conformation is controlled by ultrasonic conditions (amplitude and treatment time), and filament-based biomaterials with controllable crystallinity and degradation rate are obtained.	•SDG-7: Affordable, reliable, and sustainable access to modern energy for everyone. Target 7.a	United States	[8]
The effects of ultrasonic pretreatment on the formation of soybean protein fibrils, the interaction between soybean protein fibrils and EGCG, the rheological properties and antioxidant activities of complex and the bioaccessibility of EGCG were investigated.	•The fluorescence intensity of thioflavin T and the content of β-sheet in soybean protein fibril were higher after ultrasonic treatment, which promoted the formation of soybean protein fibril. •The stability, viscosity and antioxidant activity of soybean protein fibril treated with ultrasound assisted EGCG were improved.	•SDG-7: Affordable, reliable, and sustainable access to modern energy for everyone. Target 7.1 •SDG-12: Adopt sustainable consumption and production patterns. Target 12.2	China	[9]
The effect of ultrasonic treatment on physicochemical and functional properties was examined by pH, conductivity and solubility measurements, as well as foaming properties.	•The high temperature caused by ultrasonic treatment also decreased the conductivity of protein samples and increased the solubility and foaming capacity of whey protein.	•SDG-7: Affordable, reliable, and sustainable access to modern energy for everyone. Target 7.1 •SDG-12: Adopt sustainable consumption and production patterns. Target 12.2	Britain	[10]
Silk fibroin (SF)/polyethylene oxide (PEO) films were prepared by ultrasonic treatment before electrospinning to physically control the	•The ultrasonic treatment before electrospinning can adjust the viscosity of SF/PEO solution and	•SDG-7: Affordable, reliable, and sustainable access to modern energy for everyone. Target 7.1	Portugal	[11]

(*continued on next page*)

Table 1 (*continued*)

The Focus of the Study	Key Points	SDGs and Targets	Countries of affiliation (authors)	Reference (in the manuscript)
rheological properties of the solution and improve the spinnability of the system.	reduce the dependence of SF solution on PEO blending.			
The change of conformational structure and tensile properties of ultrasound treated silk fibroin fibers were studied by comparing the fibers with untreated ones.	•With the extension of ultrasonic treatment time, the surface oxidation effect of fibroin fibers and the transformation of random coil to β-sheet can be caused, and the strength fibers can be improved.	•SDG-7: Affordable, reliable, and sustainable access to modern energy for everyone. Target 7.1	China	[12]
The powdered microfibers and nano-fibers were obtained by ultrasonic treatment of acid aqueous solution of silk fibroin protein fibers.	•The diameter of 5–10 μm for powdered microfibers and the diameter of 30–120 nm for nanofibers can be obtained by simple and efficient ultrasonic technology.	•SDG-7: Affordable, reliable, and sustainable access to modern energy for everyone. Target 7.1	China	[13]
The cavitation effect caused by ultrasonic treatment accelerates the gelation process of silk fibroin.	•When the ultrasonic power exceeds 400 W, the gelation time of silk fibroin protein can be shortened, and the silk fibroin molecule can be transformed from random coil to β-sheet conformation.	•SDG-7: Affordable, reliable, and sustainable access to modern energy for everyone. Target 7.1	China	[14]
The ultrasonic parameters, including the output power and time, and the concentration of silk fibroin were controlled to control the gelation of silk fibroin.	•Ultrasonic treatment can control the gelation of silk fibroin protein within minutes to hours. •Ultrasound can alter the hydrophobic interaction of silk fibroin proteins and form a β-sheet structure, thus accelerating the formation of physical crosslinks responsible for gel stability.	•SDG-7: Affordable, reliable, and sustainable access to modern energy for everyone. Target 7.1 •SDG-12: Adopt sustainable consumption and production patterns. Target 12.2	United States	[15]
The hydrophilic and thermal properties of silk fibroin in wet processing and polymer modification were studied by ultrasonic treatment at different frequencies and times.	•The hydrophilicity and thermal stability of silk fibroin were improved under the condition of decreasing frequency and prolonging ultrasonic treatment time.	•SDG-7: Affordable, reliable, and sustainable access to modern energy for everyone. Target 7.1 •SDG-12: Adopt sustainable consumption and production patterns. Target 12.2	China	[16]

Note: Identifying the "key points" (column 2) will help match the SDGs addressed in the research.

in soy protein, thus enabling its potential as a drug carrier [9].

Different ultrasonic conditions have different effects on the structure and properties of biopolymer materials. Cai *et al.* [2] found that by increasing the ultrasonic power from 100 W to 800 W, the *β*-sheets content in silk fibroin protein increased from 17.39% to 20.52%, and mechanical properties increased by a factor of 2. Higuera *et al.* [3] proved that ultrasonic time may affect the solubility of whey protein [10]. Serodio *et al.* [11] found that the viscosity of silk fibroin aqueous solution increased from 1 Pa.s to 5 Pa.s by controlling the ultrasonic time of 120–330 s, thus improving the fiber forming capacity of the system. Therefore, regulating ultrasonic conditions, such as time, can result in preferred properties and a controlled structure of natural polymeric materials.

Silk fibroin protein chains exist as aggregates and micelles in the silkworm's glandular, forming a *β*-sheet structure when the silkworm spits out, with a crystallinity of about 75% [12,13]. Previous studies [1,2,14-16] found that the molecular chain of silk fibroin consist of an H-chain and an L-chain as well as a P25 protein. This factor plays a crucial role in the thermal and mechanical properties of silk. However, different preparation methods of regenerated silk fibroin may destroy its *β*-sheet structure, causing a decline of the preferred properties of the material. Therefore, study the optimal preparation methods for the regeneration of silk fibroin materials is of the upmost importance.

Similarly, soy protein isolates a globular protein derived from soybeans which are ubiquitous in nature. It can be characterized by excellent cell adhesion, metabolism, antibacterial properties, non-antigenicity, and easy absorption. Soy protein is an excellent candidate for the promotion of wound healing and tissue regeneration [17,18]. The incorporation of this highly versatile protein in this field has high potential to improve the well-being and overall health of patients worldwide. However, pure soy protein cannot be easily reconstituted into fibers due to its low moisture resistance and poor mechanical properties [19]. Therefore, to fabricate soy nanofibers, the protein is typically blended with materials conducive to improving spinnability, such as polyethylene oxide (PEO) [20] or cellulose [17] to obtain nanofiber materials. Varshney *et al.* [21] blended soy protein and silk fibroin to obtain nanofibers by electrospinning. With the addition of silk fibroin, the spinnability was improved and the mechanical properties were enhanced. Another nanofiber preparation method was proposed by Medeiros *et al.* [22], which combines electrospinning and traditional melt spinning technology. Pan *et al.* [17] blended soybean protein and chitosan in a 2:1 wt ratio and successfully spun the fiber material. Although these technologies have proved useful for applications in both the food and biomedical fields, in each of these cases the soy protein content was ususally <65%. This significantly limits the producibility and applications of soy protein-dominated fibers (such as with 80% soy proteins), which are more cost-effective and nutritious than other proteins or biopolymers. Therefore, sustainable consumption and production patterns must be implemented for successful fabrication of soy protein biofibers.

Air-jet spinning, also known as solution blow spinning [23], is a new fiber fabrication technique that addresses the drawbacks and safety concerns of electrospinning (high voltage) and melting spinning (high temperature), and is more advantageous in terms of availability of usable polymers and cost effectiveness. For this reason, air-jet spinning may be a more practical option for sustainable industrialization. This method also yields products with significantly improved productivity, with quality comparable to fibers produced by previous spinning methods.

In the present study, a soy-silk fibroin protein composite nanofiber membrane with a challenging soy/silk mass ratios of 80:20 were successfully prepared by ultrasonic assisted air-jet spinning (while other mixing ratios were also generated as controls). The performance, structural transformation and physio-biological properties of the fiber membrane materials prepared by ultrasonic spinning at different times were compared. Scanning electron microscopy (SEM), Fourier transform infrared spectroscopy (FTIR) and X-ray powder diffraction (XRD) were used to study the morphology and *β*-sheets structure of the fiber mats. Meanwhile, the thermal and mechanical properties of the composite fiber membranes were characterized by differential scanning calorimetry (DSC), thermogravimetry (TG) and dynamic thermomechanical (DMA) techniques. In addition, the hydrophilicity, stability, water

Table 2
Systematic nomenclature of SPI/SF composite fiber sample under different ultrasonic treatment times.

Abbreviated Name (in this work)	The Mixture Ratio of SPI to SF (w/w)	Ultrasonic Time (min)
IS0-30	0:100	30
IS0-60		60
IS0-120		120
IS50-30	50:50	30
IS50-60		60
IS50-120		120
IS80-30	80:20	30
IS80-60		60
IS80-120		120
IS80-180		180
IS100-30	100:0	30
IS100-60		60
IS100-120		120

retention, *in vitro* biodegradability and cytocompatibility of the composite fiber membrane were evaluated by water contact angle measurement, water retention test, enzyme degradation test and cytotoxicity test. This study provides a new strategy for the preparation of nanofiber biocomposite materials, expanding the applications of abundant natural resources for biomedicine and tissue engineering and for advancing the Sustainable Development Goals (SDGs). Table 1 summarized the examples of some research that advances the SDGs.

2. Experimental section

2.1. Raw materials

Raw materials were obtained from the following sources: Silkworm cocoons (Chinese Bombyx mori, July Trading Co., Ltd., Liaoning, China); Anhydrous $CaCl_2$ (Nanjing Wanqing Chemical Glass Co., Ltd., Nanjing, China); Anhydrous CH_3CH_2OH (Nanjing Wanqing Chemical Glass Co., Ltd., Nanjing, China); HCOOH (Nanjing Wanqing Chemical Glass Co., Ltd., Nanjing, China); Soy Protein Isolate (SPI, Beijing Ruida Henghui Technology Development Co., Ltd., Beijing, China); Ultrasonic equipment (YMNL-950Y, Nanjing Emmanuel Instrument Equipment Co., Ltd., Nanjing, China).

2.2. Fabrication of composite nanofibrous membrane

The degummed silk [24] was dissolved in a ternary solvent system of $CaCl_2/CH_3CH_2OH/H_2O$ with a molar ratio of 1:2:8, the silk fibroin solution with a concentration of 8 wt% was prepared by heating and dissolving in a 70 °C water bath. After the solution cooled to room temperature, regenerated silk fibroin (SF) was obtained after dialysis, membrane preparation and vacuum drying. Regenerated silk fibroin and soy protein isolate (SPI) were dissolved in a formic acid solvent with 4 wt% $CaCl_2$, and blended according to SPI/SF (W/W) ratios of 0/100 (IS0), 50/50 (IS50), 80/20 (IS80) and 100/0 (IS100). The protein blend solutions were stirred on a magnetic plate with a fixed total polymer concentration of 8 wt%. The SPI/SF blend was then treated with an ultrasound device consisting of a probe ultrasound source equipped with a 2 mm diameter titanium microtip. The ultrasonic power was controlled at 800 W, and the end of the ultrasonic probe was placed 10 mm below the surface of the solution for 30, 60, 120 and 180 min respectively. After ultrasonic treatment, samples were fabricated using spray spinning equipment (DQE750-24L, Dongcheng Electric Tools Co., LTD., Jiangsu, China) at room temperature with a pressure of 0.9 MPa, a spinning head diameter of 1.5 mm, and a 10 mL/h flow rate. The receiving distance was 60 cm. Finally, the soybean protein/silk fibroin composite nanofiber membrane was obtained. The theory behind solution-jet spinning nanofibers involves the high-speed stretching principle of airflow and Bernoulli's principle [25]. When the high-pressure airflow leaves the outer nozzle, the pressure decreases, the energy of the jet increases, and the velocity of the gas increases, which in turn promotes the pressure drop in the center of the jet. This forms a driving force that leads to an acceleration of the polymer solution. The high-velocity gas flow also generates shear forces at the gas/solution interface, which deforms the polymer solution from a droplet to a conical shape [25]. When this shear force overcomes the surface tension of the polymer solution, a solution jet is generated. During the flight, the solvent evaporates rapidly and the polymer is then deposited onto the collector [25].

According to the time of ultrasonic treatment, the pure silk fibroin samples were named IS0-30, IS0-60 and IS0-120, respectively (Table 2). The samples with a SPI/SF ratio of 50/50 were named IS50-30, IS50-60 and IS50-120, respectively. The samples with SPI/SF mass ratio of 80/20 were named IS80-30, IS80-60, IS80-120 and IS80-180, respectively. The names of pure soy protein are IS100-30, IS100-60, and IS100-120.

The viscosities of the Soy protein/silk fibroin solutions treated at different ultrasonic times were measured individually by DV2T cone-plate viscometer (Southeast Kechuang Technology Co., LTD. Guangzhou) A TC-650AP water bath circulation system was used to control the sample temperature at 25 °C, and the Rheocalc software was implemented for editing and data collection of the solution viscosities. The sample volumes used were 2 mL, and 12 data points were collected within a test time of 2 min.

2.3. Scanning electron microscopy

Scanning electron microscopy (SEM, JSM-7600F, JEOL, Japan) was used to examine the morphology of SPI/SF composite fiber films spun at different ultrasonic times. Conductive carbon double-sided tape was used to stick the sample on the standard sample rack, and a sputtering coating machine (JFC-1600, JEOL, Japan) was used to coat the sample with gold, the current was set to 20 mA, and each surface was plated four times at 10 s each. The working voltage of SEM was 5 kV. The samples were first moved into the sample chamber and the morphology was observed. The SEM images obtained were processed using Image J 1.53e software (National Institutes of Health, https://imagej.nih.gov/ij). This was used to analyze the porosity and fiber diameters accurately within the SEM images. The formulas implemented for average fiber diameter (D) and porosity are as it follows:

$$D = \frac{\sum_{i=1}^{i} l_i}{i} \tag{1}$$

$$Porosity(\%) = \left[1 - \left(\frac{d_{app}}{d_p}\right)\right] \times 100\% \tag{2}$$

where i is the number of fibers with diameter l_i, d_{app} is the apparent density of porous composites and d_p is the density of non-porous composites.

2.4. Fourier transform infrared spectroscopy

The FTIR spectrometer (Nicolet-Nexus 670, Nicolet, USA) was used to obtain infrared spectra of soybean protein-silk fibroin composite fiber films spun at different ultrasonic times. The sample was placed on the Ge crystal for signal collection. The resolution was 4 cm^{-1}, the scanning times were 64 times, and the spectral range was 4000–500 cm^{-1} for infrared measurement. The infrared spectra of the amide I region (1590–1710 cm^{-1}) were fitted with Gaussian curves and normalized to determine the content of secondary structures in the soy protein-silk fibroin composite fiber membrane.

2.5. X-ray diffraction analysis

X-ray diffractometer (XRD, D/MAX2500/PC, Rigaku, Japan) was

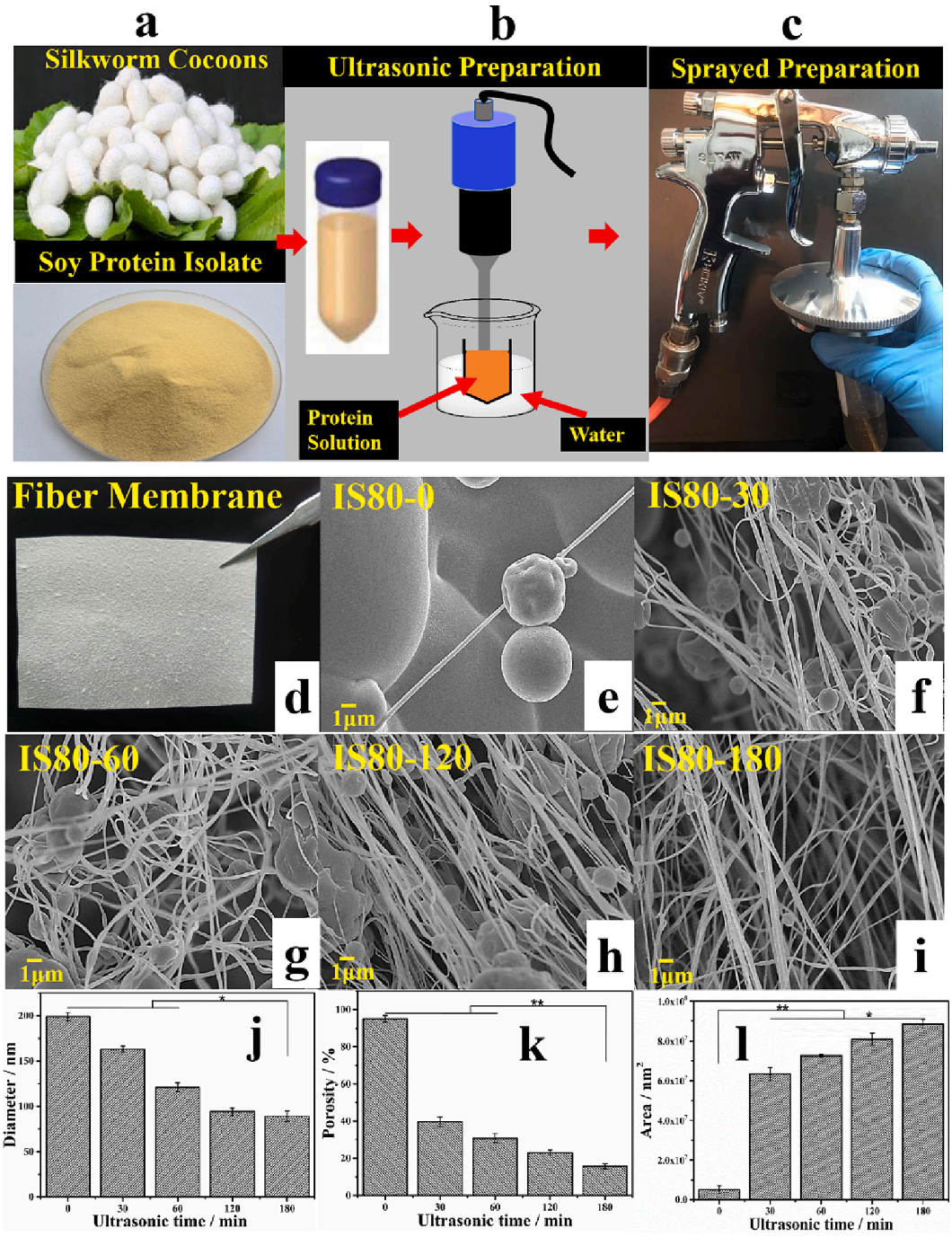

Fig. 1. Preparation flow chart of composite fiber membranes with soy protein (SPI)/silk fibroin (SF) mass ratio of 80:20 (IS80) (a-d). SEM images of the IS80 fiber membranes, spun after 0 min (e), 30 min (f), 60 min (g), 120 min (h) and 180 min (i) of ultrasound treatment. Average diameter (j), porosity (k), and surface area (l) of SPI/SF composite nanofiber membranes generated after different ultrasonic times. (Each sample size $n \geq 3$; the average diameter error is <5 nm, and error in the porosity is less than ±2%; * is $p < 0.05$; ** is $p < 0.01$).

used to obtain the XRD spectra of soybean protein-silk fibroin composite fiber films spun at different ultrasonic times. Cu Kα radiation was used with a tube pressure of 40 kV, a tube flow of 200 mA, a diffraction Angle 2θ range of 5°-60°, and a scanning rate of 10°/min.

2.6. Differential scanning calorimetry

Dried soy protein-silk fibroin composite fiber membranes were examined in a differential scanning calorimeter (DSC, Diamond TG/DTA, PerkinElmer, USA). Each sample (~4 mg) was sealed in an aluminum crucible and scanned using the conventional DSC mode in a nitrogen atmosphere at a flow rate of 30 mL/min. All empty aluminum sample trays were equipped with similar mass, with a maximum difference of ±0.1 mg. Standard mode DSC measurements were made at a heating rate of 2 °C/min. Temperature modulated differential scanning calorimetry (TMDSC) measurement was also carried out at a heating rate of 2 °C/min with a modulation period of 60 s and a temperature amplitude of ±0.318 °C. In TMDSC, the reversible heat capacity represents the reversible heat effect over the modulation temperature range.

2.7. Thermogravimetric analysis

Thermogravimetric analysis (TG, Pyris-1, PerkinElmer, USA) was used to measure changes in sample mass as temperature increases. TG curves were obtained in a nitrogen atmosphere with a gas flow rate of 50 mL/min. The samples (~3 mg) were heated from 30 °C to 550 °C at a rate of 10 °C/min. The percentage of mass change during heating was recorded. The first derivative of the mass function was obtained, showing the intermediate degradation rate of the sample.

2.8. Dynamic thermomechanical analysis

Dynamic thermo-mechanical analysis (DMA, Diamond DMA, PerkinElmer, USA) was used for mechanical testing of materials. All samples were subjected to three tests in SS tensile mode. Sample size (length × width × thickness) is 15 mm × 4 mm × 2 mm. At 25 °C, the force increases from 50 mN to 4000 mN at a rate of 500 mN/min.

2.9. Water contact angle

The surface wettability of soy protein/silk fibroin composite fiber membrane under different ultrasonic time was examined using a water contact angle meter (WCA, DSA30S, KRUSS, Germany). 2 μL of pure water was dropped on the surface of the sample for tests.

2.10. Water retention

The water retention capacity each sample was analyzed by immersing the samples in phosphate buffered saline solution (PBS) at pH 7.4 for 48 h at room temperature. At specific time points (1, 2, 4, 6, 8, 48 h), the samples were collected from the solution, excess water was removed from the surface, and each sample was weighed with a precision electronic balance (XS105 Mettle-Toled, Switzerland). Each type of samples was tested at least 3 times. Water retention percentage was determined using the following equation:

$$Waterretention(\%) = \left(\frac{W_{wet} - W_{dry}}{W_{dry}}\right) \times 100 \quad (3)$$

where W_{dry} and W_{wet} are the sample weights before and after immersing in PBS solution respectively.

2.11. Biodegradability

In order to examine the stability and biodegradation rate, samples were placed in 37 °C water, pH 7.4 PBS solution or lysozyme containing solution for 10 days. The sample residues were collected from solution at regular intervals and washed twice with distilled water, then dried and weighed on a balance. The following formula was implemented to determine the degradation percentages:

$$Degradation(\%) = \left(\frac{W_i - W_f}{W_i}\right) \times 100 \quad (4)$$

where W_i and W_f are the initial weight and the final weight of the sample respectively, that is, the weight before and after degradation.

2.12. Cytocompatibility

The biocompatibility of the soy protein-silk fibroin composite fibers was evaluated using mouse fibroblasts (L929). The samples were immersed in 75% ethanol and sterilized under UV lamp for 2 h and placed at the bottom of a 96-well plate. The preincubated L929 cells were taken out and digested with trypsin, suspended in fresh medium with 1×10^4 cells/cm^3 and added with 10% (V/V) fetal bovine serum. The cell-containing medium was inoculated on soybean protein-silk fibroin composite fiber membrane. After incubation at 37 °C and 5% CO_2 for 6, 24 and 48 h, 200 μL 0.5 mg/mL MTT solution was added and sample were incubated for 4 h. The MTT solution was then replaced with 200 μL Dimethyl sulfoxide (DMSO) and oscillated at room temperature for 10 min. The absorbance at 490 nm was measured with a microplate reader (EL-X800, BioTek, USA). Three sets of samples were tested for each sample group, and the average absorbance was measured. A control group without sample was also prepared for analysis. Cell viability was calculated by the following formula:

$$Viability = \frac{D_S}{D_C} \times 100\% \quad (5)$$

where D_s is the absorbance of the stent and D_c is the absorbance of the control.

The cells were stained with DAPI anti-fluorescence quenching agent (Baisai Biotechnology Co., Ltd., Shanghai, China), dried overnight, and then observed under a fluorescence microscopy (Nikon 80I, Nikon Instrument Co., Ltd., Shanghai, China).

3. Results and discussion

3.1. Morphology

SEM was implemented to observe the change in morphology of SPI/SF composite fiber membranes with different mass ratios after ultrasonic treatment at different times (Fig. 1, Fig. S1). As the ultrasonic time raised from 0 min to 120 min, the surface of pure soy protein sample showed many granular shapes (Fig. S1, IS100-30, IS100-60, IS100-120), while the surface of pure silk fibroin sample displayed more uniform and smooth fibers (Fig. S1, IS0-30, IS0-60, IS0-120). When the soy protein and silk fibroin were blended and sprayed at a mass ratio of 50:50, the fiber diameter was found to decrease with a more uniform morphology at an extended ultrasonic time (Fig. S1, IS50-30, IS50-60, IS50-120). Specifically, as the ultrasonic time increased from 30 min to 120 min, the average fiber diameter decreased from 176 nm to 101 nm for IS0 (silk) samples, and from 188 nm to 155 nm for IS50 samples (Fig. S1j); the porosity also decreased from 26.22% to 8.82% for IS0, and from 13.62% to 8.82% for IS50 (Fig. S1k).

However, with the higher soy protein content in sample IS80-0 (80%) (Fig. 1e), many beads appeared and nanofibers could not be obtained. This is suggested to stem from the low viscosity of the solution. The spray spinning process involves a large number of droplets to form, affecting the stretching of the jet solution to form fibers. As the ultrasonic time increased from 30 min (Fig. 1f) to 180 min (Fig. 1I), the beads gradually decreased until they eventually disappeared (Fig. 1I). The fiber diameter (Fig. 1j) and porosity (Fig. 1k) also decreased as the fiber surface area increased (Fig. 1l): the fiber diameter decreased from 199 nm (IS80-0) to 89 nm (IS80-180); and the porosities decreased from 95.1% (IS80-0) to 15.7% (IS80-180). The viscosity of the spinning solution increased after ultrasonic treatment, suggesting a potential improvement of the fiber morphology without the presence of beading. The number of fibers per unit area increased, thus reducing the porosity between the fibers. This result was consistent with the study by Serôdio *et al.* [11]. Droplets form when the viscoelasticity of the solution is too small to resist deformation caused by surface tension during spinning. Beading was observed at a low viscosity while smooth bead-free fibers were observed at a high viscosity [25]. Therefore, the fiber surface area gradually increased from 5.17×10^6 nm^2 (IS80-0) to 8.85×10^8 nm^2 (IS80-180). At extended ultrasonic treatment times, the viscosity of the solutions increased, and the diameter of the spun fibers decreased (Fig. S2). These findings prove that the ultrasonic time can significantly affect the fiber surface morphology and fiber sizes. In addition, studies have shown that nanofibers with high soy protein contents are more conducive to cell growth, migration, and vitality, making them extremely useful in the field of biomedicine [19,21]. Since the results demonstrated that soy protein-dominated nanofibers (e.g. IS80) can

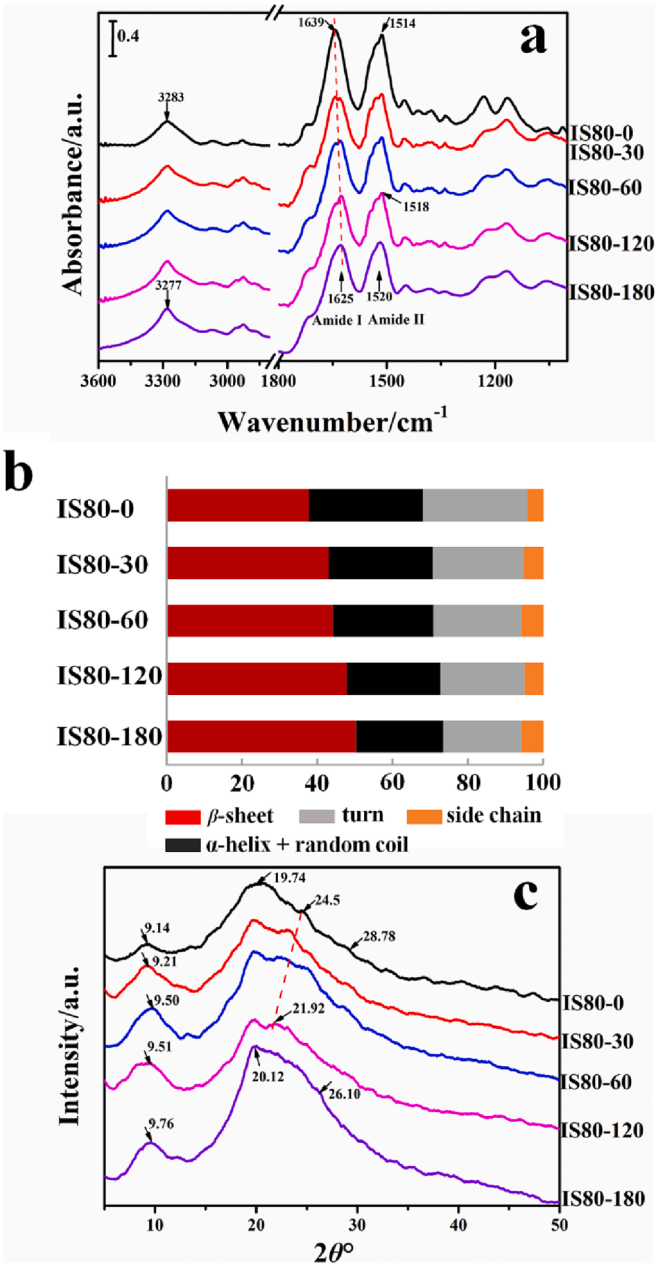

Fig. 2. ATR-IR spectra of the soy protein-silk fibroin nanofiber samples at different ultrasonic times in the wavelength range of 3600–1000 cm^{-1} (a), FTIR fitting diagram of secondary structure content of composite nanofiber membranes (b), and XRD spectra of composite nanofibers in the range of 2θ = 5-50° (c).

only be fabricated through this ultrasound-assisted method, we extended the study of 80/20 soy-silk composite fiber membranes, and investigated their structural and property changes under different ultrasonic times.

3.2. Structural analysis

The 80:20 soy protein/silk fibroin composite fiber membranes obtained by jet spinning after ultrasonication for different times were studied using FTIR (Fig. 2a) to investigate the changes in protein structure. Ultrasonic cavitation produces a local heat and energy that improves the mobility of peptide chains and the crystal transition of the protein. Table S1 summarized the relationship between ultrasonic treatment time and the temperature of SPI/SF composite solutions. The amide I region mainly signifies C = O stretching vibrations of protein structures. Protein has different secondary structures, including β-sheets (1616–1637 cm^{-1}), random coils (1638–1655 cm^{-1}), α-helix (1656–1662 cm^{-1}), β-turns (1663–1696 cm^{-1}) and side chains (1605–1615 cm^{-1}). Therefore, FTIR can be used for quantitative analysis of the secondary structure in the protein [26-29]. The bands in the amide II region (1600–1500 cm^{-1}) are mainly due to the inverse combination of C-N stretching and N-H bending vibrations [30]. The amide N region (3310–3270 cm^{-1}) is ascribed to the stretching vibrations of N-H and O-H [2]. For the IS80 protein composite fiber membrane, their peak positions gradually change with the ultrasonic time from 0 to 180 min: the peaks were found to shift from 1639 cm^{-1} (IS80-0) to 1625 cm^{-1} (IS80-180), from 1514 cm^{-1} (IS80-0) to 1520 cm^{-1} (IS80-180), and from 3283 cm^{-1} (IS80-0) to 3271 cm^{-1} (IS80-180). The peak intensity of amide I region was found to increase and become sharper as the ultrasonic treatment time increased. This phenomenon was also noted by Wang *et al.* [12] in a study on the ultrasonic treatment of silk fibroin from 0 to 60 min. This indicated that the longer ultrasonic times enhance the hydrogen bond interactions between protein molecular chains.

The FTIR Amide I spectra were then curve-fitted (Fig. S3) to further analyze the secondary structures in the soy-silk fibroin system [2,31,32]. As shown in Fig. 2b, all of the samples showed a high content of β-sheets, and with the increase of sonication time, the β-sheets content increased from 37.77% (IS80-0) to 50.237% (IS80-180). The α-helical content and random coils decreased from 30.19% (IS80-180) to 23.12% (IS80-180), the content of turns decreased from 27.75% (IS80-0) to 20.90% (IS80-180). These results prove quantitatively that the soy-silk protein composite fibers prepared by ultrasonic jet spinning promoted the structural transition from random coils/helix to β-sheets conformation and enhances hydrogen bond interactions with increasing of ultrasonic treatment times [2].

This relationship was further examined using XRD. In the XRD curves (Fig. 2c), the peak at 2θ of 9.14° for the unsonicated samples (IS80-0) corresponded to α-helix. The characteristic peaks at 19.74° and 24.5° correspond to β-sheets structure, and the peaks at 28.78° correspond to random coils. After ultrasonic treatment, the peak intensity and position of composite changed. For example, as the ultrasonic time increased, the characteristic peak shifted from 9.14° (IS80-0) to 9.76° (IS80-180). The characteristic peak of sample IS80-0 at 24.5° gradually shifted to the left, causing the peak near 20° to sharpen. This trend was seen again for the peak at 28.78° (IS80-0), which decreased gradually and moved left to 26.10° (IS80-180). These examples together indicate that longer ultrasonic treatment times will cause the random coil structure in SPI/SF composite nanofibers to transform into a β-sheets conformation [12,30-33]. The resulting changes of peak position, peak strength, peak shape and the secondary structure contents all indicate that an extension of ultrasonic time enhance the hydrogen bond interactions between soy and silk fibroin proteins as well as causing an increase in the β-sheet crystal content.

3.3. Thermal analysis

The DSC results of the IS80 composite nanofibers prepared by air spinning at different ultrasonic times are shown in Fig. 3a. The results presented here show that the SPI/SF nanofibers contain two endothermic peaks: an endothermic peak around 100 °C which corresponds to the moisture volatilization of the sample during heating, and two endothermic peaks (Table 3, T_{p1} and T_{p2}) in the range of 250–360 °C attributed to the decomposition process of random coil/helix and β-sheet structures of the protein composites, respectively [34,35]. As the ultrasonic treatment time increased, the peak temperature T_{p1} increased from 284.56 °C (IS80-0) to 293.54 °C (IS80-180). The peak temperature T_{p2} increased from 339.55 °C (IS80-0) to 349.68 °C (IS80-180). This suggests that the intermolecular hydrogen bond interactions can be intensified with increasing ultrasonic treatment time, raising the

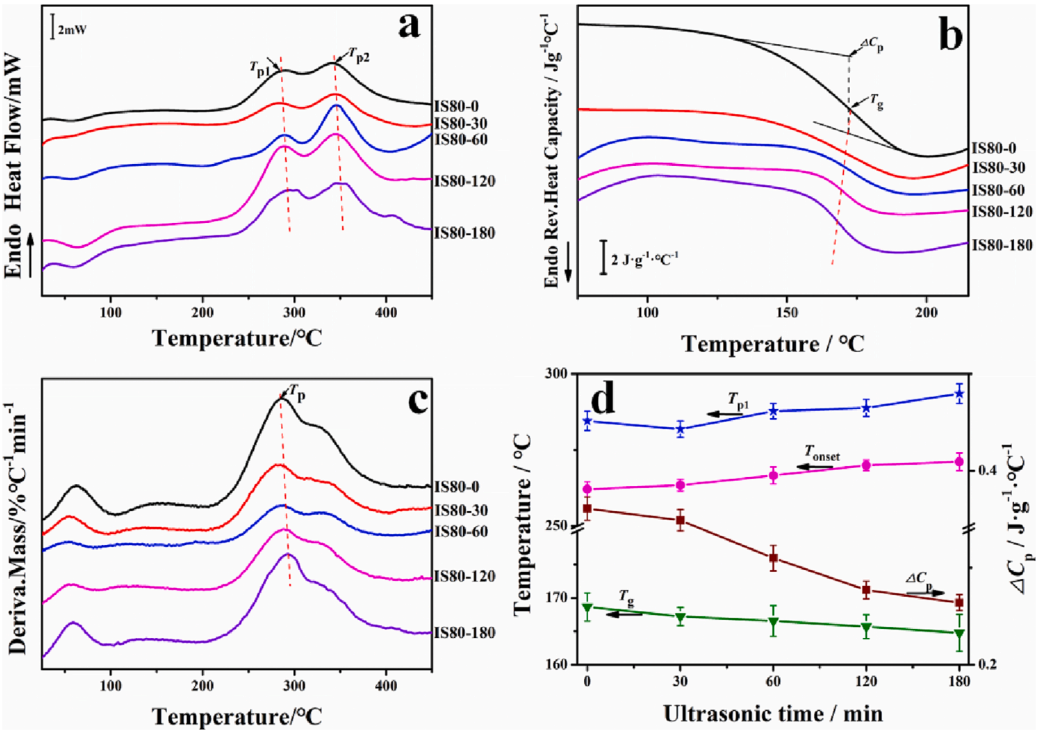

Fig. 3. DSC curves of soy protein/silk fibroin nanofibers at different ultrasonic times (a), TM-DSC curves (b), DTG curves (c), and numerical changes of thermodynamic parameters (d). The initial thermal decomposition temperature T_{onset} is derived from the TGA curve (Fig. S4).

Table 3
Thermal and mechanical properties of ultrasonic jet spun soy protein/silk fibroin composite nanofibers.

Sample	T_{p1}/°C	T_{p2}/°C	T_{onset}/°C	T_p/°C	m/%	T_g/°C	ΔC_p	Modulus/MPa	Strength/MPa	Elongation/%
IS80-0	284.56±0.63	339.55±0.44	262.11±0.38	285.62±0.29	35.87	168.64±0.28	0.361±0.011	2.04±0.07	0.801±0.03	46.46±0.83
IS80-30	281.82±0.44	342.58±0.51	263.45±0.82	286.50±0.38	32.21	167.23±0.79	0.349±0.008	5.4±0.04	1.484±0.07	58.97±0.49
IS80-60	287.77±0.73	345.13±0.47	266.60±0.76	288.18±0.32	27.7	166.55±0.63	0.310±0.013	7.21±0.12	2.358±0.21	82.37±1.02
IS80-120	288.82±0.57	346.13±0.65	269.94±0.59	288.57±0.46	23.3	165.70±0.55	0.277±0.003	9.8±0.17	3.646±0.15	85.41±0.76
IS80-180	293.54±0.81	349.68±0.58	271.11±0.72	293.06±0.54	16.9	164.79±0.89	0.264±0.017	21.65±0.09	3.981±0.25	89.16±0.50

T_{p1} and T_{p2} are the degradation peak temperatures of silk fibroin-soy protein nanofibers from the DSC curve, respectively. ΔC_p is the specific heat capacity on the DSC curve. The initial thermal decomposition temperature T_{onset} and the maximum weight loss rate peak temperature T_p are derived from the TGA curve. T_g is the glass transition temperature obtained by TMDSC. Modulus, Strength and Elongation are derived from the DMA curve, represent materials elastic modulus, ultimate strength and elongation ratio, respectively. Each sample group were tested at least 3 times.

decomposition temperature of protein structures and thus improving the compatibility and stability.

To further investigate the IS80 composite nanofibers at different ultrasonic times, the glass transition process of the samples was determined by TMDSC technology. Fig. 3b presents a plot of the reversible heat capacity curve of the sample between −20 – 250 °C. The glass transition temperature (T_g, Table 3) was determined by locating the midpoint of the reversible heat capacity step, and the step exhibited by the sample in the glass transition region is the heat capacity (ΔC_p, Table 3) [19]. The TMDSC plots show that all samples only have one glass transition in the range of 75–220 °C, and the glass transition temperature gradually decreased with increasing ultrasonic time (Fig. 3d). This suggests that the SPI/SF composite system was still a homogeneous system. The T_g was shown to decrease from 168.64 °C (IS80-0) to 164.79 °C (IS80-180). ΔC_p was found to decrease from 0.361 J·g^{-1}·°C^{-1} for IS80-0 to 0.264 J·g^{-1}·°C^{-1} for IS80-180 (Fig. 3d). The decrease of ΔC_p suggests that the β-sheet crystalline content of the system increases with increasing sonication time. Other studies [8,13,14,36] have also determined that long-term ultrasonic treatment can transform the random coil protein structure into a stable β-sheet structure. These findings are consistent with our findings that ultrasonic time influences the transformation of the secondary structures in SPI/SF materials.

The thermogravimetric analysis shows the thermogravimetric change (Fig. S3) and thermogravimetric rate (Fig. 3c) of the IS80 nanofiber samples at different ultrasonic times in the range of 30–550 °C. From 30–120 °C, weight loss occurs in the sample as the water evaporates off with increasing temperature [19]. With the increasing sonication time, the initial decomposition temperature (T_{onset}, Table 3) gradually increased from 262.11 °C for IS80-0 to 271.11 °C for IS80-180 (Fig. 3d). The TG results indicate a high thermal stability of SPI/SF nanofibers as ultrasonic treatment time increases.

3.4. Mechanical property analysis

Fig. 4a presents the stress-strain curves for the IS80 composite nanofibers prepared by jet spinning at different ultrasonic times. To demonstrate a model of the swelling conditions in a standard biological environment, the samples were first soaked in deionized water at 37 °C for 10 min before DMA testing. At least three tests were performed for each type of samples (n ≥3), and the mechanical parameters such as elastic modulus and elongation ratio were calculated (Table 3). The elastic modulus is a critical parameter to evaluate the ability of an object to resist elastic denaturation. The elongation ratio reflects the ductility

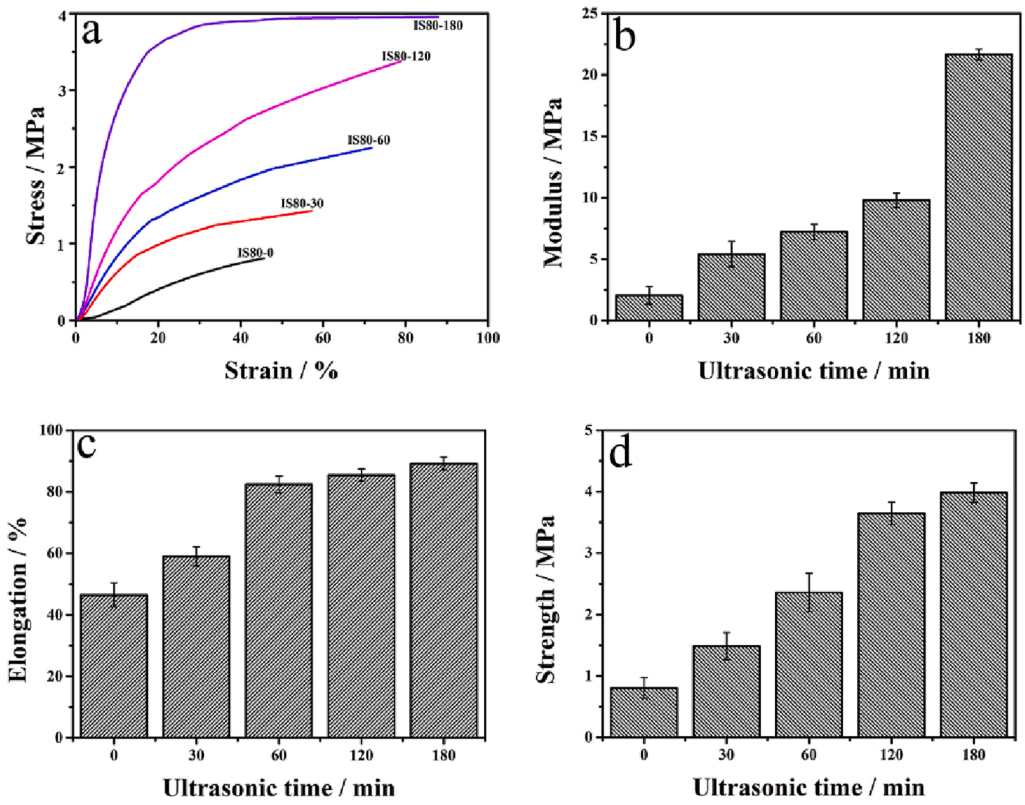

Fig. 4. Stress-strain curves of the SPI/SF nanofiber samples at different ultrasonic times (a). And elastic modulus (b), elongation ratio (c), and ultimate strength of composite fiber membranes (d).

of the material and the bonding strength between molecules in blended samples [2,19]. As seen in Fig. 4b, the elastic modulus increased from 2.04 MPa (IS80-0) to 21.65 MPa (IS80-180) with increasing sonication time. The ultimate strength increased from 0.801 MPa (IS80-0) to 3.981 MPa (IS80-180), as seen in Fig. 4c. Several studies have also found that the tensile strength of fiber is determined by its β-sheets crystalline structures [12]. The strength and elongation of a material are usually inversely proportional. The stronger a material, the worse its elongation is. However, in the present work, it was found that both elongation ratio and strength were greatly improved with increasing sonication time. This was suggested to be due to the arrangement of protein molecular chains [2]. Ultrasonic treatment may cause the non-crystalline region of the protein chains to form a more ordered orientation. With increasing ultrasonic treatment times, the chain orientation and the degree of crystallization will both increase. Additionally, with increasing ultrasonic time, the molecular interaction between the proteins was enhanced, leading to better elasticity in the samples. With longer ultrasonic times, the fibers were thinner, and the porosity in each sample is the smaller. Therefore, the composite nanofibers sonicated for 180 min exhibited the best strength and also displayed the highest elasticity.

3.5. Hydrophilicity and water retention property

In addition to the need for considerable mechanical properties, the optimal material for biomedical applications most importantly possesses excellent biocompatibility and hydrophilicity. The hydrophilicity/hydrophobicity of the material can be best examined by water contact angle measurements [37]. Studies have shown that pure silk fibroin films are hydrophobic due to their carboxyl, amino, hydroxyl and three-dimensional nanofibrous structures [2]. Soy protein contains 58% polar amino acids, making it hydrophilic [21]. This makes the addition of SPI to silk an excellent candidate to improve the surface wettability of fiber membrane. In Fig. 5a, the water contact angle for the unsonicated sample (IS80-0) was 89.1°. With increasing ultrasonic treatment time, the water contact angle gradually decreased from 77.1° (IS80-30) to 57.3° (IS80-180) (Fig. S5). This is due to the rearrangement of protein molecules caused by ultrasonic treatment. Longer ultrasonic times promote hydrophilic segments to appear on the surface of the material [15,16], increasing the hydrophilicity of SPI/SF nanofibers.

The IS80 nanofiber sample was placed in the aqueous solution at room temperature. The mass change of the sample was studied at different time intervals ranging from 0 to 48 h to investigate the water retention capacity of the composite nanofiber membrane. As shown in Fig. 5b, the weight of the composite fiber membrane changed greatly from 0 to 6 h. At 6 h, the weight of the composite fiber membrane increased from 152.68% (IS80-0) to 232.71% (IS80-180) with increasing ultrasonic times. After 48 h, the weight change trend of the samples was IS80-180 > IS80-120 > IS80-60 > IS80-30 > IS80-0. Thirugnanaselvam *et al.* [38] argued that that sonication could reduce the moisture vapor transmission rate (MTVR) of soy protein membranes and control the exudation of tissue fluid from wounds at an optimal rate. This was confirmed in the present study, as a prolonged ultrasonic treatment caused a decreased in the SPI/SF nanofiber diameter, a decreased in porosity, and an increased in surface area. All these factors are attributed to a greater water retention capacity in nanofibers.

3.6. Biodegradability

To evaluate nanomaterials biostability and biodegradability for biomedical applications [19], the IS80 nanofibers were soaked in water, PBS buffer, and lysozyme solution for 10 days. Each sample group was first presoaked in water for 6 h to reach its maximum weight increase due to water retention (Fig. 5), then soaked in the different solutions and massed at different time intervals. Results show an improved degradability of the composite fiber materials with prolonged ultrasonic treatment times. When degraded in aqueous solution (Fig. 6a) for 10

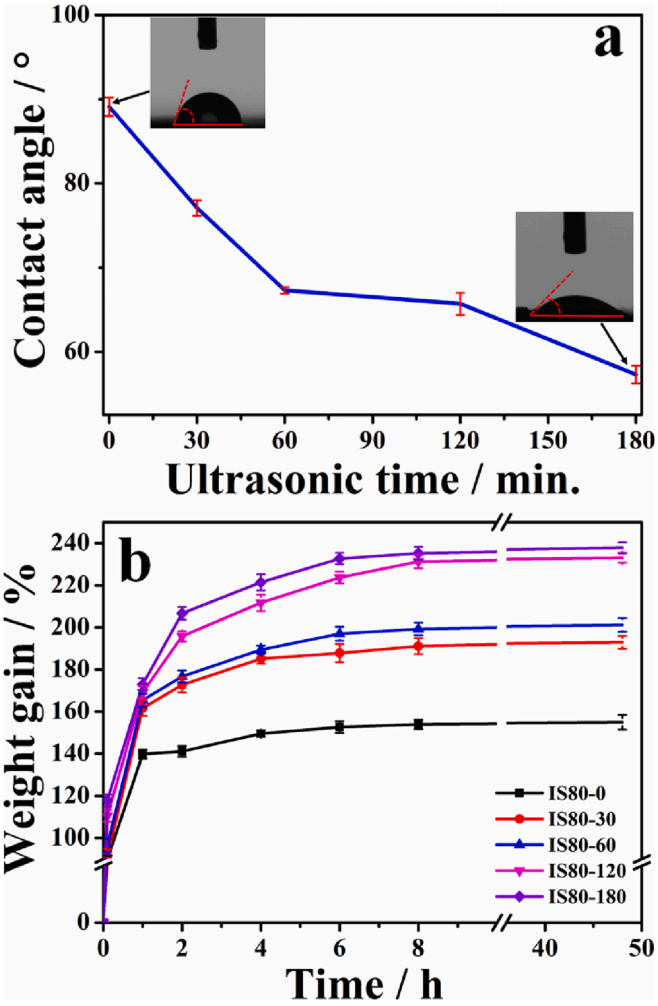

Fig. 5. Water contact angle diagram of SPI/SF nanofibers prepared by ultrasonic jet spinning (a), and weight change curves in aqueous solution at 25 °C for 0–48 h (b). Each data reported is the average of three trials. The significant statistical differences were observed between the samples ($p < 0.05$).

days, the sample weight loss increased from 3.76% (IS80-0) to 8.75% (IS80-180). In the PBS buffer solution (Fig. 6b), the sample weight loss increased from 5.56% (IS80-0) to 13.27% (IS80-180). Fig. 6c depicts the *in vitro* degradation using lysozyme buffer solution. It was found that in the first 24 h with increasing ultrasonic time, the degradation rate of the SPI/SF samples increased. The IS80-180 sample had the highest degradation rate of up to 17.95%. On the 10th day, the weight loss of sample IS80-0 was 19.71%, and the weight loss of sample IS80-180 reached 58.35%. These findings prove that the enzymatic degradation rate of fibrous membranes is influenced by changes in morphology, microstructure, and molecular orientation [2,8,9,12]. For example, through a series characterization experiments based on structural and performance of SF casting films under different ultrasonic power and time treatment, Cai *et al.* [2] found that the ultrasound could increase the gaps between nanoparticles. The study demonstrated an increase in the intermolecular β-sheets and α-helix contents, leading the silk to be insoluble in water with both mechanical strength and flexibility. Additionally, Wang *et al.* [12] investigated silk at different ultrasonic times in a chemical free environment to illustrate that a transformation of random coil to β-sheet within the secondary structure and the local intensive pressure and heat produced by acoustic cavitation during ultrasonic treatment led to an increase of carbonyl groups and oxygen content on the surface of the fiber. Countless other studies have demonstrated that the enzymatic degradation process and biological

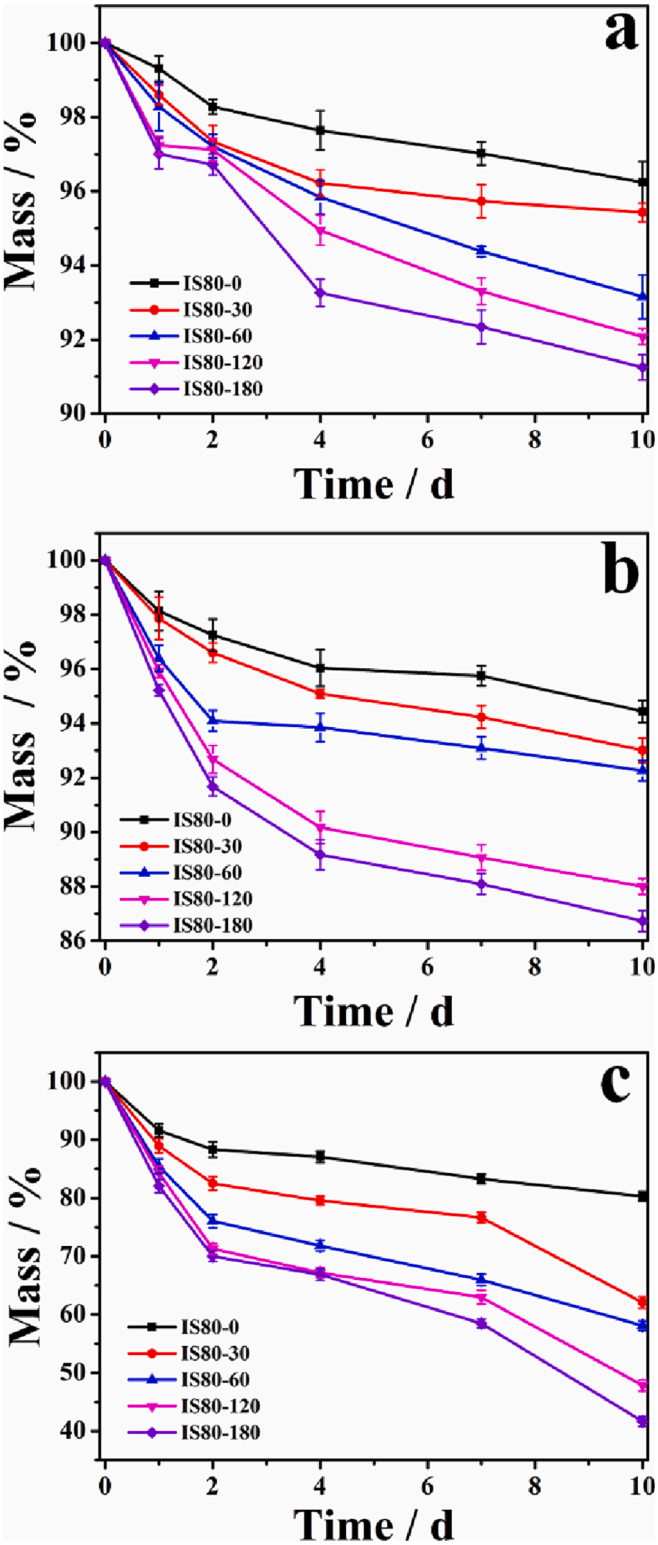

Fig. 6. Biodegradation of SPI/SF nanofiber samples prepared by jet spinning at different ultrasonic times: in water (a), PBS buffer (b), and lysozyme buffer solution (c).

stability may be related to the structure, surface morphology and intermolecular interactions of polymer chains [2,39-44]. For instance, one study [2] found that the gas permeability increased for the silk protein under the ultrasonic action, which could promote cell adhesion, differentiation and growth within samples. This is due an increase in the gap between the molecular chain segments, exposing more hydrophilic

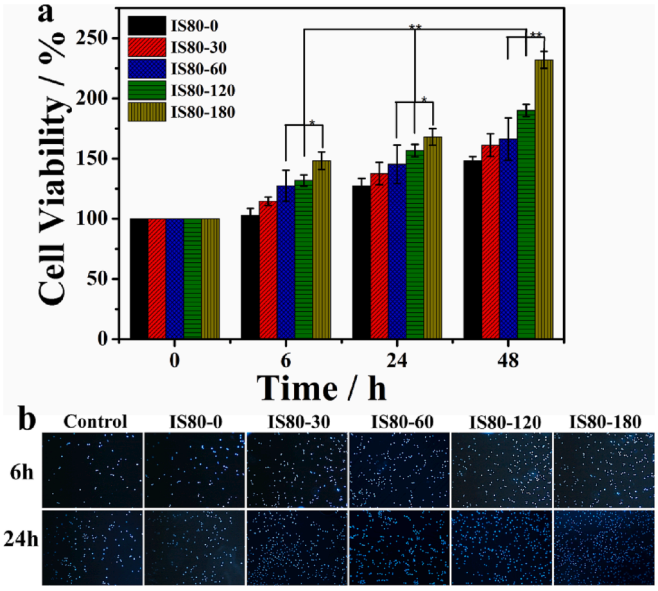

Fig. 7. Histogram of viability of mouse fibroblasts (L929) attached to composite fibrous membrane samples under different sonication times after 0, 6, 24 and 48 h, using glass surface as control (* $p < 0.05$, ** $p < 0.01$) (a), cells stained with DAPI and observed using an upright fluorescence microscope after 6 h and 24 h (b).

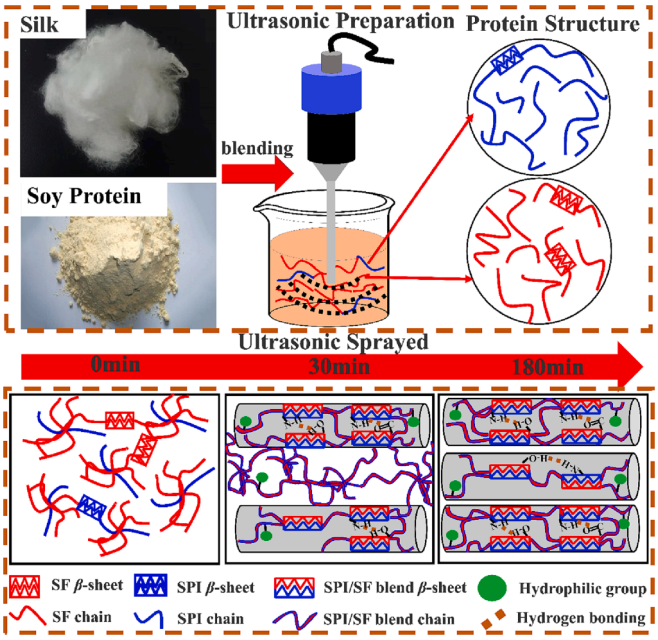

Fig. 8. Diagram of the mechanism of ultrasonic air-jet spun SPI/SF nanofibers.

groups. Baran *et al.* [40] detected that the cell area and length were sensitive to the variations of morphology and conjugate of fibroin and chitosan composition. The same study also found that it was resistant to the degradation by protease and lysozymes, caused by a limited availability of the starch chains to the enzyme's active site after an extensive crosslinking between the aldehydes of starch and the primary amino groups provided mainly from chitosan matrix.

3.7. Cytocompatibility

Mouse fibroblasts (L929) were used for *in vitro* cytotoxicity experiments to evaluate the biocompatibility and cell viability of SPI/SF nanofiber samples. Fig. 7 shows the effect of different ultrasonic times (IS80-0, IS80-30, IS80-60, IS80-120, IS80-180) of the IS80 nanofiber samples cultured with mouse fibroblasts at 6, 24, and 48 h. The cell viability on all composite membranes showed an increasing trend with the cultured time. Specifically, the cell viability of sample IS80-0 cultured for 6 h, 24 h and 48 h was 102.78%, 127.46% and 148.23%, respectively. As ultrasonic treatment time increased, the cell viability on SPI/SF nanofibers also increased. The cell viability of the IS80-180 sample was the most notable. The sample IS80-180 reached respective viabilities of 148.23%, 168.01% and 231.97%. These results suggest that SPI/SF composite nanofibrous membranes can contribute to cell adhesion and growth, especially when treated with longer sonication times. Similarly, different surface micropatterns have been discussed to control cell growth and proliferation on biopolymer blend films [44]. Dong *et al.* [45] found that cell growth and adhesion were improved with decreasing surface particle size of zein membranes. Cai *et al.* [46] and Wang *et al.* [47] discovered that the high hydrophilicity of the material was more conducive to cell adhesion, growth, and proliferation. The result of this study additionally proves that smaller fiber diameters and a larger fiber specific surface area is more favorable for cell adhesion and growth. This is closely related to the ultrasonic treatment of the SPI/SF membranes at different times.

In addition, to test the cytocompatibility of SPI/SF composite fibrous membranes prepared by jet spinning after ultrasonication for different times, cells were stained on the surface of the samples. As shown in Fig. 7b, the morphology of the cells on the IS80 nanofibers remained stable for 6 and 24 h after the cells were seeded on the samples, indicating that all SPI/SF fibers support cell growth. When the sample was inoculated with cells for 6 h, the composite fibrous membrane after ultrasound was more efficient at promoting cell attachment, growth and proliferation. It was observed that the cell density was proportional to the ultrasound time. A significant increase in cell density was also observed with increasing sonication time after 24 h of placement, suggesting that an increase of ultrasonic time promotes smaller fiber diameters with larger surface areas for favorable cell growth.

3.8. Mechanism of ultrasound on air-jet spinning nanofibers

In general, there is a competition between the stress of the polymer solution and its surface tension that is guided by the solution properties and processing parameters. Three forms were spun out: droplets, beads-on-string, and uniform fibers [25]. Low viscoelasticity causes an inability of the polymer to resist deformation from the surface tension. This causes the formation of droplets. When the Rayleigh instability is sufficiently suppressed by fiber formation, uniform fibers will form. After the stabilization of fibers between droplets from the entangled polymer networks partially resist the Rayleigh instability, the beads-on-string structure will form [25]. Therefore, the spinnability of polymer solutions is suggested to primarily be determined by the relationship between surface tension and viscoelasticity [8,9,18,20,22]. Ewaldz *et al.* [25] pointed out that viscoelastic stresses and microstructural transitions could alter free surface flows in complex fluids. Morphological and rheological studies on electrospun polymer solutions found that the high-surface-tension solvents require increased extensional viscosities and relaxation times to form smooth fibers [10,20,25]. Jet-spinning has become the new frontrunner in manufacturing technology for ultrafine fibers, with a similar mechanism to electrospinning, although the pulling force in the case of jet-spinning is provided from gas.

Based on our results, we envisioned the following mechanism (Fig. 8) to illustrate the effect of air jet-spinning with different ultrasonic treatment times on the structural, thermal, mechanical, and biological properties of SPI/SF nanofibers. Since the polymer solution underwent the flow and extension forces during spinning [10,25], the viscosity of the spinning solution was increased with the extension of the ultrasonic time. This promoted smooth fiber formation in high-surface-tension solutions, enhanced the stability of the jet, and increased the surface

Table 4
Comparison of properties between the biomaterials obtained in this work and those from sources cited in literature.

Materials*	Applications	Properties			Refs.
		Degradati on (the Mass loss)	Mechanical properties	Cell viability	
SF hydrogel	Tissue engineering	~80% after 4 days.	the strain: 5–10%	maintained for several weeks.	[8]
SF film	Tissue engineering	~74.3% after 3 days	the strength: 19.13Mpa.	~150% after 72 h	[2]
SF-chitosan film	Tissue engineering	~50% after one week	improved	improved	[38]
SF-PLA foam film	Biomedical science	~30% after 6 days	improved	~115% after 72 h	[41]
SF-SP film	Tissue engineering	~30% after 10 days	the elasticity: 15.28 MPa the elongation: 39.34%	~140% after 48 h.	[19]
SF-SP nanofiber film (this study)	Biomedical, Tissue engineering	~58.35% after 10 days	the strength: 21.65 MPa the elongation: 89.16%.	~231.97% after 48 h	In our work

* The abbreviation SF, PLA and SP in the materials column stands for silk fibroin, polylactic acid and soy protein, respectively.

tension required at a higher polymer concentration. Additionally, ultrasonic treatment led to an increased solubility. Besides, with the extension of treatment times, the segments could be rearranged in a more orderly manner. Samal *et al.* [8] elucidated that the energy input from ultrasonication might cleave the longer chains to generate hydrogen and hydroxyl radicals. The radicals could be recombined to return to their original form or new forms, such as sol-gel transitions. The results of their study suggested that increased exposure times of sonication could make the random coil state of SF protein convert to stable β-sheet structures. The work of Cai *et al.* [2] also showed that ultrasonic treatment could increase the crystallinity of silk protein in casting film, reducing the agglomeration of SF fibers. Since the elongation at break is determined by the arrangement of protein molecular chains, they also confirmed that the sample elongation gradually increases with the increase of ultrasonic time, which helps a part of the amorphous region of SF chain form a more ordered direction. Therefore, for a sample with a high spherical protein content, e.g. IS80, the heat from continuous ultrasound treatment could provide enough energy for the recombination of protein molecules in the spinning solution, thus enhancing the interactions between silk fibroin and spherical soy protein. Overall, this supported the formation of more ordered structures when a thin jet of solution was emitted. The incorporation of sonication lead to an increase of the solubility and viscosity due to the intermolecular interactions, forming fibers under the competitive affection from stress-strain and surface tension that occurred during spray spinning. FTIR analysis in our work illustrated that the content of β-sheets was increased and the content of α-helix and random coil was decreased. The mechanical properties of the material were considerably improved, causing the strength and elongation of the samples to increase with sonication time. In addition, the β-sheets content of the SPI/SF nanofiber membrane increased with longer ultrasonic times, enhancing the interaction between the two protein molecules such as forming hydrogen bonds between N-O, C = O or O-H groups in silk fibroin and soy proteins. Ultrasonic treatment is suggested to lengthen the space between the protein molecular segments, exposing more hydrophilic groups on the surface of the material. The enhanced water absorption and cytocompatibility of the samples were promoted cell adhesion and growth. Previous works [8-10] were consistent with our findings. For example, Tong *et al.* [9] showed that ultrasonic treatment could improve rheological properties and antioxidant activity of soy protein by unfolding of soy protein structure and exposure of hydrophobic regions. Additionally, Serôdio *et al.* [10] proved that ultrasonic treatment significantly improved the average viscosity of SF/polyethylene oxide solutions and improved the quality of spun fibers. Overall, our air spun fiber results demonstrated that increased sonication times cause structural transformations and improve various physical and biological properties of protein nanofibers compared to unsonicated samples. In comparison with other biomaterials cited in literature (Table 4), the biomaterials developed within this study have the potential to become excellent candidates in several biomedical and tissue engineering applications.

4. Conclusion

In this work, we have established a novel method of fabricating soy-silk fibroin protein composite nanofiber membranes by ultrasonic jet spinning at different times and successfully obtained protein composite nanofibers with different morphologies and properties. Through several characterization methods, the structural transformation and physico-biological properties of the materials pretreated by ultrasound were studied. SEM analysis showed that with the prolongation of ultrasonic time, the composite nanomaterials exhibited small fiber diameter and low porosity, establishing a high surface area to improve the spinnability of the composite materials. FTIR and XRD analysis showed that increase of ultrasonic time enhanced the intermolecular interactions and promoted the transformation of the material structure from random coils to β-sheets conformation. Their thermal properties were also examined with DSC, TGA and DMA techniques. Results confirmed that prolonged ultrasonic time will improve the thermal stability, hydrophilicity, water retention and enzymatic degradation rate of composites. These enhanced properties by sonication helped improve the cell adhesion on the composite nanomaterials, while providing a favorable environment for the proliferation of fibroblast cells on the nanofiber surface. All these factors indicate soy-silk protein nanofibers to be a suitable candidate for tissue regeneration, wound dressings or drug delivery systems. A molecular model was proposed to explain the effect of ultrasonic treatment on the material. This model could serve as a basis for ultrasound as a new tool to tune the structure and properties of air-jet spun materials for use in the biological and sustainable chemistry fields.

Declaration of Competing Interest

The authors declare that they have no known competing financial interests or personal relationships that could have appeared to influence the work reported in this paper.

Data availability

Data will be made available on request.

Acknowledgements

This study is supported by the National Natural Science Foundation of China (21973045). J.M. and X.H. are supported by Rowan University Seed Research Grants, and the US NSF Future Manufacturing Program (CMMI-2037097).

Appendix A. Supplementary data

Supplementary data to this article can be found online at https://doi.org/10.1016/j.ultsonch.2023.106341.

References:

[1] S.J. Eom, N.H. Lee, M.C. Kang, Y.H. Kim, T.G. Lim, K.M. Song, Silk peptide production from whole silkworm cocoon using ultrasound and enzymatic treatment and its suppression of solar ultraviolet-induced skin inflammation, Ultrasonics Sonochemistry 61 (2020), 104803.

[2] B.W. Cai, H.L. Gu, F. Wang, K. Printon, Z.G. Gu, X. Hu, Ultrasound regulated flexible protein materials: Fabrication, structure and physical-biological properties, Ultrasonics sonochemistry 79 (2021), 105800.

[3] O.A. Higuera-Barraza, C.L.D. Toro-Sanchez, S. Ruiz-Cruz, E. Marquez-Rios, Effects of high-energy ultrasound on the functional properties of proteins, Ultrasonics Sonochemistry 31 (2016) 558–562.

[4] B.W. Cai, J. Mazahreh, Q.Y. Ma, F. Wang, X. Hu, Ultrasound-assisted fabrication of biopolymer materials: A review, International Journal of Biological Macromolecules 209 (2022) 1613–1628.

[5] H. Hu, I.W.Y. Cheung, S.Y. Pan, C.Y. Eunice, L. Chan, Effect of high intensity ultrasound on physicochemical and functional properties of aggregated soybean β-conglycinin and glycinin, Food Hydrocolloids 45 (2015) 102–110.

[6] S.X. Xu, Q. Wu, J. Wu, H.K. Huamin, Y.J. Zhu, C.Q. Ning, K.R. Dai, Ultrasound-assisted synthesis of nanocrystallized silicocarnotite biomaterial with improved sinterability and osteogenic activity, Journal of Materials Chemistry B 8 (15) (2020) 3092–3103.

[7] S. Bera, D. Mondal, A role for ultrasound in the fabrication of carbohydrate-supported nanomaterials, Journal of Ultrasound 22 (2) (2019) 131–156.

[8] S.K. Samal, D.L. Kaplan, E. Chiellini, Ultrasound sonication effects on silk fibroin protein, Macromolecular Materials and Engineering 298 (11) (2013) 1201–1208.

[9] X. Tong, J. Cao, T. Tian, B. Lyu, L.M. Miao, Z.T. Lian, W.Y. Cui, S. Liu, H. Wang, L. Z. Jiang, Changes in structure, rheological property and antioxidant activity of soy protein isolate fibrils by ultrasound pretreatment and EGCG, Food Hydrocolloids 122 (2022), 107084.

[10] A.R. Jambrak, T.J. Mason, V. Lelas, Z. Herceg, I.L. Herceg, Effect of ultrasound treatment on solubility and foaming properties of whey protein suspensions, Journal of food engineering 86 (2) (2008) 281–287.

[11] R. Serôdio, S.L. Schickert, A.R. Costa-Pinto, J.R. Dias, P.L. Granja, F. Yang, A. L. Oliveira, Ultrasound sonication prior to electrospinning tailors silk fibroin/PEO membranes for periodontal regeneration, Materials Science and Engineering: C 98 (2019) 969–981.

[12] W.C. Wang, H.F. Long, L. Chen, Y.Q. Liu, Q. Li, Ultrasonics induced variations in molecular structure and tensile properties of silk fibers in a chemical free environment, Nano Select 2 (10) (2021) 1962–1967.

[13] H.Y. Wang, Y.Y. Chen, Y.Q. Zhang, Processing and characterization of powdered silk micro- and nanofibers by ultrasonication, Materials Science and Engineering: C 48 (2015) 444–452.

[14] Y.Y. Wang, Y.D. Cheng, Y. Liu, H.J. Zhao, M.Z. Li, The Effect of Ultrasonication on the Gelation Velocity and Structure of Silk Fibroin, Advanced Materials Research 175 (2011) 143–148.

[15] X.Q. Wang, J.A. Kluge, G.G. Leisk, D.L. Kaplan, Sonication-induced gelation of silk fibroin for cell encapsulation, Biomaterials 29 (8) (2008) 1054–1064.

[16] W.C. Wang, L.J. Rather, K. Gong, Q. Zhou, T.H. Zhang, Q. Li, Effects of Ultrasonic Treatment on Hydrophilicity and Thermal Stability of Silk, Macromolecular Materials and Engineering 304 (12) (2019) 1900364.

[17] Y.J. Pan, X.J. Huang, X.W. Shi, Y.F. Zhan, G. Fan, S.Y. Pan, J. Tian, H.B. Deng, Y. M. Du, Antimicrobial application of nanofibrous mats self-assembled with quaternized chitosan and soy protein isolate, Carbohydrate Polyms 133 (2015) 229–235.

[18] P. Dorishetty, R. Balu, A. Sreekumar, L.d. Campo, J.P. Mata, N.R. Choudhury, N.K. Dutta, Robust and tunable hybrid hydrogels from photo-cross-linked soy protein isolate and regenerated silk fibroin, ACS Sustainable Chemistry & Engineering 7 (10) 9257-9271.

[19] F.T. Yang, B.W. Cai, H. Heng, H.L. Gu, F. Wang, Preparation, structure and properties of soy protein and silk fibroin composite nanofiber membrane by jet sponning, Science China Chemistry 52 (05) (2022) 709–720.

[20] X.Z. Xu, L. Jiang, Z.P. Zhou, X.F. Wu, Y.C. Wang, Preparation and properties of electrospun soy protein isolate/polyethylene oxide nanofiber membranes, ACS Appl Mater Interfaces 4 (8) (2012) 4331–4337.

[21] N. Varshney, A.K. Sahi, S. Poddar, S.K. Mahto, Soy protein isolate supplemented silk fibroin nanofibers for skin tissue regeneration: Fabrication and characterization, International Journal of Biological Macromolecules 160 (2020) 112–127.

[22] E.S. Medeiros, G.M. Glenn, A.P. Klamczynski, W.J. Orts, L.H.C. Mattoso, Solution blow spinning: A new method to produce micro-and nanofibers from polymer solutions, Journal of applied polymer science 113 (4) (2009) 2322–2330.

[23] P.K. Sow, R. Singhal, Sustainable approach to recycle waste polystyrene to high-value submicron fibers using solution blow spinning and application towards oil-water separation, Journal of Environmental Chemical Engineering 8 (2) (2020), 102786.

[24] F. Wang, S.S.J. Aravind, H. Wu, J. Forys, V. Venkataraman, K. Ramanujachary, X. Hu, Tunable green graphene-silk biomaterials: Mechanism of protein-based nanocomposites, Materials Science and Engineering: C 79 (2017) 728–739.

[25] E. Ewaldz, J. Randrup, B. Brettmann, Solvent Effects on the Elasticity of Electrospinnable Polymer Solutions, ACS Polymers Au 2 (2022) 108–117.

[26] M.A. Souza, J.E. Oliveira, E.S. Medeiros, G.M. Glenn, L.H.C. Mattoso, Controlled release of linalool using nanofibrous membranes of poly (lactic acid) obtained by electrospinning and solution blow spinning: a comparative study, Journal of nanoscience and nanotechnology 15 (8) (2015) 5628–5636.

[27] X.P. Zhuang, L. Shi, K.F. Jia, B.W. Cheng, W.M. Kang, Solution blown nanofibrous membrane for microfiltration, Journal of membrane science 429 (2013) 66–70.

[28] H.L. Wang, X. Zhang, N. Wang, Y. Li, X. Feng, Y. Huang, C.S. Zhao, Z.L. Liu, M. H. Fang, G. Ou, H.J. Gao, X.Y. Li, H. Wu, Ultrahigh–current density anodes with interconnected Li metal reservoir through overlithiation of mesoporous AlF3 framework, Science advances 3 (9) (2017) e1701301.

[29] Y.J. Jiang, C. Li, X. Nguyen, S. Muzammil, E. Towers, J. Gabrielson, Qualification of FTIR spectroscopic method for protein secondary structural analysis, Journal of pharmaceutical sciences 100 (11) (2011) 4631–4641.

[30] F. Wang, H.Y. Yu, Z.G. Gu, S. Ling, Q.C. Liu, X. Hu, Impact of calcium chloride concentration on structure and thermal property of Thai silk fibroin films, Journal of Thermal Analysis and Calorimetry 130 (2) (2017) 851–859.

[31] X. Hu, K. David, C. Peggy, Determining beta-sheet crystallinity in fibrous proteins by thermal analysis and infrared spectroscopy, Macromolecules 39 (18) (2006) 6161–6170.

[32] D. Badillo-Sanchez, D. Chelazzi, R. Giorgi, A. Cincinelli, P. Baglion, Understanding the structural degradation of South American historical silk: A Focal Plane Array (FPA) FTIR and multivariate analysis, Scientific reports 9 (1) (2019) 1–10.

[33] X. Wang, M. Majzoobi, A. Farahnaky, Ultrasound-assisted modification of functional properties and biological activity of biopolymers: A review, Ultrasonics Sonochemistry 65 (2020), 105057.

[34] A.M. Herrero, F. Jiménez-Colmenero, P. Carmona, Elucidation of structural changes in soy protein isolate upon heating by Raman spectroscopy, International journal of food science & technology 44 (4) (2009) 711–717.

[35] M. Yao, D. Su, W. Wang, X. Chen, Z. Shao, Fabrication of air-stable and conductive silk fibroin gels, ACS applied materials & interfaces 10 (44) (2018) 38466–38475.

[36] H.C. Wu, F.W. Shen, X. Hong, W.V. Chang, H. Winet, Monitoring the degradation process of biopolymers by ultrasonic longitudinal wave pulse-echo technique, Biomaterials 24 (22) (2003) 3871–3876.

[37] Q.Q. Deng, F. Wang, C.R. Gough, X. Hu, Tunable microphase-regulated silk fibroin/poly (lactic acid) biocomposite materials generated from ionic liquids, International Journal of Biological Macromolecules 197 (2022) 55–67.

[38] M. Thirugnanaselvam, N. Gobi, S.A. Karthick, SPI/PEO blended electrospun martrix for wound healing, Fibers and Polymers 14 (6) (2013) 965–969.

[39] F.L. Mi, Y.M. Lin, Y.B. Wu, S.S. Shyu, Y.H. Tsai, Chitin/PLGA blend microspheres as a biodegradable drug-delivery system: phase-separation, degradation and release behavior, Biomaterials 23 (15) (2002) 3257–3267.

[40] E.T. Baran, K. Tuzlakoglu, J.F. Mano, R.L. Reis, Enzymatic degradation behavior and cytocompatibility of silk fibroin–starch–chitosan conjugate membranes, Materials Science and Engineering: C 32 (6) (2012) 1314–1322.

[41] F. Wang, H. Liu, Y.Y. Li, Q.Y. Ma, J. Zhang, X. Hu, Tunable Biodegradable Polylactide-Silk Fibroin Scaffolds Fabricated by a Solvent-Free Pressure Controllable Foaming Technology, ACS Applied Bio Materials 3 (12) (2020) 8795–8807.

[42] F. Wang, H.Y. Yu, Q.C. Liu, Q.Y. Ma, Z.G. Gu, Structure and Kinetics of Thermal Decomposition Mechanism of Novel Silk Fibroin Films, Acta Physico-Chimica Sinica 33 (2) (2017) 344–355.

[43] P.R. Sivashankari, M. Prabaharan, Three-dimensional porous scaffolds based on agarose/chitosan/graphene oxide composite for tissue engineering, International journal of biological macromolecules 146 (2020) 222–231.

[44] F. Wang, H. Wu, V. Venkataraman, X. Hu, Silk fibroin-poly(lactic acid) biocomposites: Effect of protein-synthetic polymer interactions and miscibility on material properties and biological responses, Materials Science and Engineering: C 104 (2019), 109890.

[45] J. Dong, Q. Sun, J.Y. Wang, Basic study of corn protein, zein, as a biomaterial in tissue engineering, surface morphology and biocompatibility, Biomaterials 25 (19) (2004) 4691–4697.

[46] K.Y. Cai, K.D. Yao, S.B. Lin, Z.M. Yang, X.Q. Li, H.Q. Xie, T.W. Qing, L.B. Gao, Poly (D, L-lactic acid) surfaces modified by silk fibroin: effects on the culture of osteoblast in vitro, Biomaterials 23 (4) (2002) 1153–1160.

[47] B.B. Wang, H.M. Lou, H.L. Xu, J.P. Zhao, Q.J. Wang, Q. Shi, Y.H. Deng, High voltage, solvent-free solid polymer electrolyte based on a star-comb PDLLA–PEG copolymer for lithium ion batteries, RSC advances 8 (12) (2018) 6373–6380.